WallGen, Software to Construct Layered Cellulose-Hemicellulose Networks and Predict Their Small Deformation Mechanics[1]

Hung Kha, Sigrid C. Tuble, Shankar Kalyanasundaram, and Richard E. Williamson*

Department of Engineering, College of Engineering and Computer Science (H.K., S.C.T., S.K.), and Research School of Biology, College of Medicine, Biology, and Environment (H.K., S.C.T., R.E.W.), Australian National University, Canberra 0200, Australia

We understand few details about how the arrangement and interactions of cell wall polymers produce the mechanical properties of primary cell walls. Consequently, we cannot quantitatively assess if proposed wall structures are mechanically reasonable or assess the effectiveness of proposed mechanisms to change mechanical properties. As a step to remedying this, we developed WallGen, a Fortran program (available on request) building virtual cellulose-hemicellulose networks by stochastic self-assembly whose mechanical properties can be predicted by finite element analysis. The thousands of mechanical elements in the virtual wall are intended to have one-to-one spatial and mechanical correspondence with their real wall counterparts of cellulose microfibrils and hemicellulose chains. User-defined inputs set the properties of the two polymer types (elastic moduli, dimensions of microfibrils and hemicellulose chains, hemicellulose molecular weight) and their population properties (microfibril alignment and volume fraction, polymer weight percentages in the network). This allows exploration of the mechanical consequences of variations in nanostructure that might occur in vivo and provides estimates of how uncertainties regarding certain inputs will affect WallGen's mechanical predictions. We summarize WallGen's operation and the choice of values for user-defined inputs and show that predicted values for the elastic moduli of multinet walls subject to small displacements overlap measured values. "Design of experiment" methods provide systematic exploration of how changed input values affect mechanical properties and suggest that changing microfibril orientation and/or the number of hemicellulose cross-bridges could change wall mechanical anisotropy.

Plant scientists have long studied how primary wall structure influences mechanical properties (Preston, 1974). In this work, we develop methods to predict the elastic modulus for layered networks of cellulose microfibrils (CMFs) cross-linked by hemicellulose (HC) chains when they are subject to small imposed displacements.

Polysaccharides provide over 90% of wall mass and therefore are likely to dominate wall mechanics. Two distinct but probably interacting (Zykwinska et al., 2005) networks are recognized: a cellulose-hemicellulose (CHC) network and a pectin network. Pectins can be removed by mutations, allowing measurements of the mechanical properties of the CHC network (Ryden et al., 2003) that can be compared with predicted values. The two networks probably make roughly comparable mechanical contributions in pectin-rich dicots (Ryden et al., 2003), but the CHC network presumably dominates in monocots with pectin-poor, type II walls (Carpita and Gibeaut, 1993; Rose, 2003). Plant cells align CMFs (Baskin, 2005) but not noncellulosic polysaccharides such as pectins and HCs. CMF alignment, therefore, underlies the structural and mechanical anisotropy seen in many cell walls.

In principle, wall structure can predict mechanical properties, a multiscale modeling problem of the type that materials scientists often tackle (Kwon et al., 2008). In this context, structural and mechanical inputs concern polymer chains or aggregates, and mechanical properties are predicted for pieces of material several orders of magnitude larger that contain many polymer chains. There are some structure-based quantitative predictions of the mechanics of secondary walls (Bergander and Salmén, 2002; Keckes et al., 2003; Salmén, 2004; Hofstetter et al., 2005; Altaner and Jarvis, 2008), but most discussions of primary walls only involve qualitative consideration of how factors such as CMF length and alignment might change growth anisotropy (Wasteneys, 2004; Baskin, 2005) rather than the small displacement mechanical properties with which we are concerned. Modeling plant cell walls provides several particular challenges. First, walls vary greatly in CMF alignment, with multinet, polylamellate, helicoidal, and other types recognized; second, polymer composition varies even within one wall type; and third, polymer interactions remain un-

[1] This work was supported by the Australian Research Council (grant no. DP0665069) and the Research School of Biological Sciences.

* Corresponding author; e-mail richard.williamson@anu.edu.au.

The author responsible for distribution of materials integral to the findings presented in this article in accordance with the policy described in the Instructions for Authors (www.plantphysiol.org) is: Hung Kha (hung.kha@anu.edu.au.).

www.plantphysiol.org/cgi/doi/10.1104/pp.109.146936

certain, with the view that HCs cross-bridge CMFs (Hayashi, 1989) challenged on various grounds by those regarding them as providing spacing or otherwise facilitating movement between CMFs (Whitney et al., 1999; Thompson, 2005). In beginning multiscale modeling of primary walls, therefore, we sought a strategy that facilitated in silico experiments in which we could vary the structure, composition, and other wall properties that contribute to the complex microstructure of cell walls and that provided the opportunity to give the polymers more complex properties in future studies.

Many modeling strategies facilitate computation by simplifying (homogenizing) wall structure by aggregating the properties of many polymers. Procedures are well established but do not obviate the necessity to understand the underlying polymer properties and impose an additional requirement to deduce the properties of the population being homogenized. Cell walls are often compared with fiber composites, for which several approaches to the prediction of the elastic properties have been reported (Chamis and Sendeckyj, 1968). Most such micromechanical approaches, however, are based on simplifying assumptions about the geometry of the microstructure or special relations between the phase properties. Moreover, although cell walls are often described as fiber composites, this obscures important distinctions, notably the difference between the continuous interfiber matrix typical of most manufactured fiber composites and the discrete HC cross-links present in the cell wall. The mechanical properties of the continuous matrix are relatively easily measured for manufactured fiber composites, but replacing HC cross-bridges with a continuous matrix requires defining its mechanical properties. Various micromechanical models of secondary walls assume that a homogenous HC matrix surrounds CMFs (Bergander and Salmén, 2002; Salmén, 2004; Hofstetter et al., 2005); for example, Hofstetter et al. (2005) gave this phase a bulk modulus taken from testing an isotropic HC powder. Increased computing power now provides the option to avoid such homogenization with at least three advantages accruing. First, homogenization often limits the ease with which different structures can be investigated (a high priority issue for us), since homogenization assumptions may need to be reexamined and recalibrated as microstructure changes. Without homogenization, a wide range of structures can be analyzed, given that a flexible system is available for generating microstructure. Second, accumulating knowledge of the mechanics of individual polymer chains coming from techniques such as atomic force microscopy can be directly applied to the individual HCs and CMFs in a nonhomogenized model. If homogenization is applied, that relationship is lost and new assumptions must be made about the properties of the population. Third, once the basic model is established, the properties of the polymers, particularly those of the HCs, can be varied to more accurately capture the nonlinear and other properties seen on extension.

We avoided homogenization by using the WallGen program to build a fragment of virtual wall whose components have one-to-one spatial and mechanical correspondence with the CMFs and HCs of a primary wall CHC network. We chose finite element analysis (FEA) to predict the mechanical properties of the entire fragment containing thousands of CMFs and HCs. In effect, then, WallGen averages by setting up the most realistic spatial arrangement, using mechanical data for individual chains and leaving FEA to predict the collective properties. The well-established engineering technique of FEA has been used to predict wall mechanics at cellular and subcellular scales. Examples include predicting cell response to microindentation (Bolduc et al., 2006) or compression between flat plates (Smith et al., 1998) and predicting the mechanics of pulped fiber networks in paper (Hansson and Rasmuson, 2004). These applications have not involved mechanical representation of individual wall polymers, but FEA has been used at this scale to model individual microtubules and F-actin polymers pulling on membranes (Allen et al., 2009) and at even finer scales to model tubulin lattice deformation within single microtubules (Schaap et al., 2006). Modern FEA programs have features of potential value for developing more sophisticated models of wall mechanics: components can have nonlinear force-extension properties and viscoelastic properties, and conditions can be specified to break links between components of the microstructure. This should allow exploration of the more complex mechanical behavior that CHC networks show when subject to larger displacements and incorporation of additional mechanical elements providing the properties generated by pectins.

In this article, we describe how WallGen operates, review the choice of values for several important inputs, predict the elastic moduli of multinet walls in which HCs cross-link CMFs, compare those values with experimental values, and quantify the mechanical effects of varying several inputs to the virtual wall. We restrict consideration to polymers given linear elastic properties and, because small strains are sufficient to predict the elastic modulus, restrict experiments to small displacements to minimize inaccuracies from this simplification. A previous publication considered issues relating to representative volume elements and analyzed some simpler CHC networks (Kha et al., 2008).

RESULTS

WallGen Operations

Overview

WallGen uses a stochastic self-assembly mechanism to construct the CHC network of a virtual wall fragment containing numerous CMFs and HCs and having dimensions comparable to the dimensions of a small cell. The wall has two types of interlinked beam

elements with dimensions, spatial distribution, and mechanical properties designed for one-to-one correspondence with CMFs and HCs in a real wall. FEA of the network predicts its mechanical properties. User-defined inputs (Table I) apply to single polymer chains (HCs) or polymer aggregates (CMFs) and define either individual structural and mechanical properties (dimensions, M_r, elastic moduli) or population properties (alignment, CMF volume fraction [VF], each polymer's percentage contribution by weight to the network).

The flow chart (Fig. 1) summarizes WallGen's operations. WallGen constructs the virtual wall by placing CMFs in layers and connecting them into a three-dimensional network with in-layer and inter-layer HCs (Fig. 2). It identifies sites where HCs and CMFs intersect as nodes for FEA and connects the nodes with the appropriate beam elements. The beam elements represent a CMF if nodes share the same CMF or an HC if they share the same HC but different CMFs (Fig. 3A). HyperWorks, acting as a preprocessor for FEA, assigns mechanical properties, including elastic modulus and Poisson ratio, to the beam elements. Abaqus (a FEA code) models the mechanical response to an enforced displacement (Fig. 3B) from which the elastic moduli of the entire wall fragment are calculated.

Table I. *Some of the major user-defined inputs to WallGen*

The inputs given as examples will construct a sheet of multinet wall that is 9.6 × 9.6 μm, with four layers of CMFs, and subject it to a displacement of 40 nm in a direction perpendicular the mean alignment of microfibrils in layer 1.

Inputs
Dimensions of the wall fragment
No. of layers: 4
Layer separation (nm): 26
Length along *x* axis (nm): 9,600.0
Length along *y* axis (nm): 9,600.0
Settings for mechanical testing
Constraints direction: 2
Displacement (nm): 40.0
Properties of CMFs and XGs
CMF VF: 0.015
Weight % CMF: 64.0
CMF thickness (nm): 3.2
CMF width (nm): 3.2
CMF length mean (nm): 6,000.0
CMF length SD (nm): 0.01
CMF ends minimum separation (nm): 30.0
Weight % XG: 36.0
Molecular mass of XG (kD): 400.0
XG thickness (nm): 0.5
XG width (nm): 0.5
XG length (nm): 260.0
CMF orientations in each layer
Layer 1
CMF mean orientation (rad): 1.57
CMF SD for orientation (rad): 0.1
Layer 2
CMF mean orientation (rad): 1.57
CMF SD for orientation (rad): 0.2
Layer 3
CMF mean orientation (rad): 1.57
CMF SD for orientation (rad): 0.3
Layer 4
CMF mean orientation (rad): 1.57
CMF SD for orientation (rad): 1.5

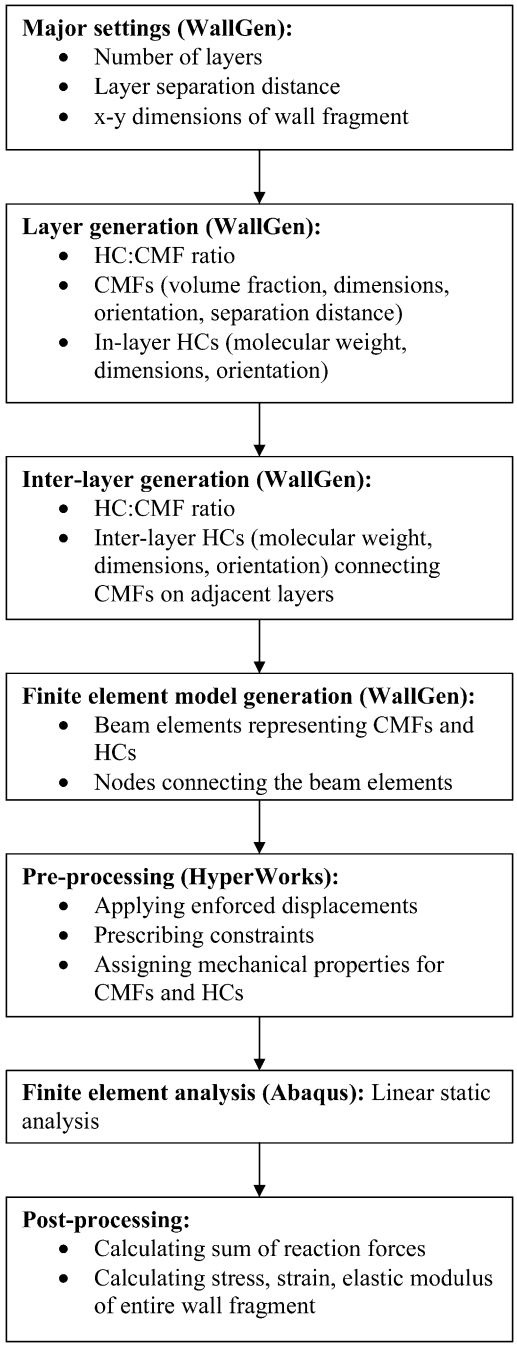

Figure 1. Flow chart summarizing the operation of WallGen and the mechanical analysis of the structures it generates.

Initial Settings

The user fixes the size of the wall fragment by specifying the lengths of its edges in the *x*-*y* plane and

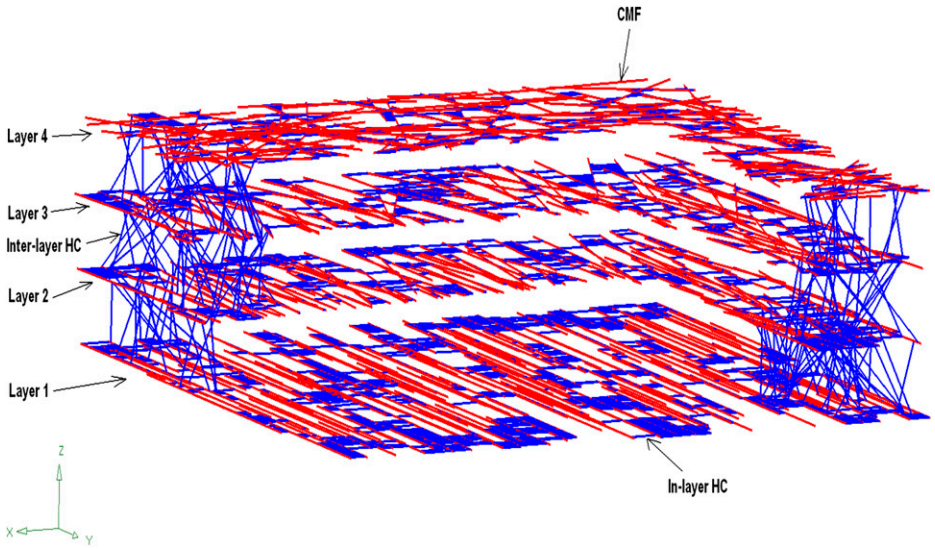

Figure 2. Cut-away view showing the arrangement of the virtual CHC network WallGen assembles ready for FEA. CMFs are arranged in layers and are connected into a three-dimensional network by in-layer and inter-layer HCs. For clarity, interlayer HCs are only shown in two small areas. The wall has a multinet arrangement of CMFs, with nearly parallel alignment in layer 1 (adjacent to the plasma membrane) transforming gradually to a random arrangement in layer 4.

its thickness along the *z* axis specified as the number of CMF layers and the distance separating adjacent layers. The first and last layers of CMFs are considered to define the surfaces of the virtual wall in calculating wall thickness.

CMF Generation

WallGen uses the dimensions (length, width, thickness) of CMFs and the volume of the wall to calculate how many CMFs must be deposited to achieve the VF (total CMF volume/total wall volume). The target number for the CMFs in each layer is calculated from this total number. CMFs are generated singly in each layer: midpoints are positioned randomly in *x-y* space, and ends are then positioned to provide lengths and orientations that the user specifies as means ± SD. Orientation is specified separately for each layer. WallGen rejects a new CMF if either of its ends is too close to the ends of any preexisting CMFs. This provides some spacing but allows CMFs in the virtual wall to cross in the way that electron micrographs suggest occurs in the real wall (Lai-Kee-Him et al., 2002). WallGen shortens any CMFs protruding beyond the edges of the fragment by giving them a new end placed where the original CMF left the fragment.

HC Generation

Once enough CMFs have been generated in each layer to meet the wall's target VF, WallGen calculates the mass of cellulose present in the virtual wall. It uses the total length of CMFs deposited and assumes that each CMF has 36 parallel glucan chains and each glucan chain contains 2 anhydroglucose units per nm. WallGen uses this figure for the mass of cellulose together with the HC M_r (user defined) to determine how many HC molecules will give the wall its user-defined weight percentage for HCs. The program partitions the total number of HC chains equally between in-layer and inter-layer HC arrays to give a target number of molecules for each array. Each HC is assumed to form a single cross-bridge only, which is experimentally supported for low M_r HC (Pauly et al., 1999) but may underestimate the number formed by HC with higher M_r.

WallGen first places in-layer HCs, giving them midpoints at random sites in the layer's *x-y* space and ends positioned in plane to provide the user-specified length. The latter sets the maximum cross-bridge length in the final wall and so should not exceed the contour length for a HC polymer with the chosen M_r. After each HC chain has been generated, WallGen only accepts it if it intersects two CMFs in that layer (Fig. 3A). The rejection technique is adapted from a method to determine the connectivity of fibers in models of cement boards and other materials (Stahl et al., 1997; Stahl and Kramer, 1998). The orientation of HC molecules in *x-y* space can be aligned or left random (when some weak alignment may still arise because the assembly process may discriminate against HCs running parallel to CMFs and so failing to intersect with them). Once all layers have the target number of cross-bridging HCs, WallGen generates the target number of HCs in each inter-layer array to produce a three-dimensional network (Fig. 2). HC centers are generated at random sites in the *x-y* plane situated midway between adjacent wall layers. Ends are generated according to the specified length and, although HC orientations can be controlled, HCs are usually allowed to form in a range of orientations relative to the *z* axis (Fig. 2). As with in-layer HCs, WallGen rejects any newly generated HC not contacting a CMF in each of the two adjacent layers and continues generating further HCs until the target number of HCs is achieved.

Connectivity

When CMF and HC generation are completed, WallGen determines their intersection points and con-

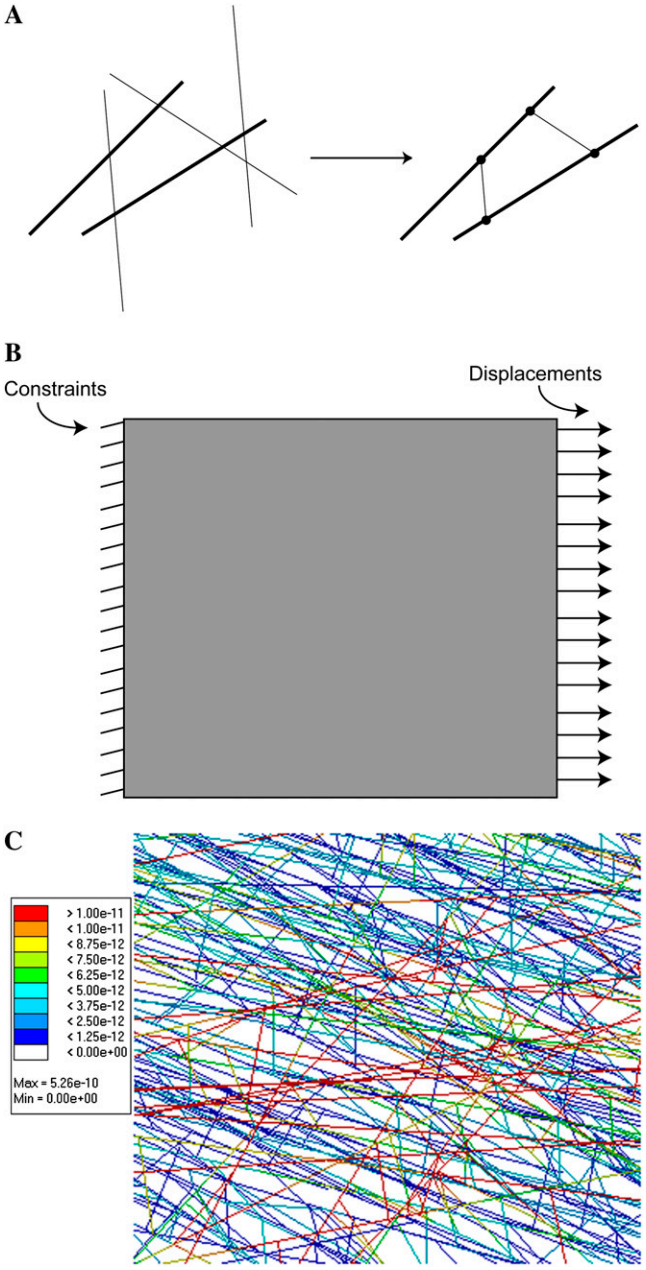

Figure 3. Assembling, displacing, and analyzing stresses in the CHC network. A, WallGen first deposits CMFs and HCs (thick and thin lines, respectively). It identifies sites where HCs and CMFs intersect as nodes for FEA (circles) and connects the nodes with the appropriate beam elements representing either a CMF if they share the same CMF or an HC if they share the same HC. HCs that do not intersect two CMFs are rejected during WallGen's operations. B, The preprocessor HyperWorks applies enforced displacements to nodes lying along one side of the wall fragment while constraining nodes lying along the wall's opposite edge. C, The magnitude of stresses (N nm^{-2}) in each mechanical element in the network is resolved during the FEA and color coded according to magnitude. CMFs in layer 1 were oriented along the *y* axis, and the enforced displacement was along the *x* axis. Components in all four layers are seen.

nectivity. Every CMF is checked against every HC to locate intersection points. These are designated as nodes for FEA, and the identification numbers of the CMF and HC that meet at each node are stored. The program then creates a series of CMF-type beam elements, with each beam element extending between successive nodes involving the same CMF. Once the CMF beam elements have been created, WallGen finds intersection points that use the same HC but different CMFs. A beam element of the HC type is created as a cross-bridge between the intersection points on the neighboring CMFs (Fig. 3A). Parts of the HC initially projecting beyond the intersection points on the CMFs are omitted from the cross-bridging HC beam element. These are regions of HC that would hydrogen bond to the CMF surface or be buried within the CMF in the real wall (Hayashi, 1989).

Mechanical Analysis

The preprocessor (Hyperworks) applies an enforced displacement in the plane of the appropriate layer to the nodes down one edge of the wall fragment while constraining the nodes along the opposite edge (Fig. 3B). All other nodes are free to move in *x*, *y*, and *z* planes and to rotate. Abaqus (a FEA code) models the network's mechanical response to the enforced displacement using a linear static analysis. The elastic modulus of the entire wall fragment is calculated by dividing the stress (ratio between reaction forces on the nodes having enforced displacements and the fragment's cross-sectional area) by the strain (ratio between the enforced displacements and the original fragment length). The magnitude of the stress carried by each CMF and HC in the network can be resolved (Fig. 3C) and shows considerable heterogeneity depending on, among other factors, orientation relative to the direction of the imposed displacement.

Choosing Input Values

CMF Dimensions

CMFs that are several micrometers long are readily liberated from various slime-rich walls and measured by electron microscopy (Franke and Ermen, 1969; Sprey and Bochem, 1993), but the drastic treatments required for release from walls with conventional CHC networks raise doubts about whether those released CMFs retain their in vivo lengths. Atomic force microscopy of pectin-depleted walls (Davies and Harris, 2003) show CMFs that are 3.2 nm thick, consistent with them containing single crystallites whose sizes have been estimated by NMR and x-ray diffraction (Kennedy et al., 2007b).

CMF VF

To provide spatial correspondence between CMFs and HCs in virtual and real walls, we specify cellulose

per unit of wall volume rather than per unit of wall mass, which is usually favored for chemical analyses. VF is a common parameter in materials science and in early cell wall studies, but it has been less widely used recently in describing cell walls, so our estimates come from reported CMF spacings. Estimated spacings were 30 nm in onion (*Allium cepa*) parenchyma walls prepared by rapid-freeze, deep-etch electron microscopy (McCann et al., 1990; McCann and Roberts, 1991) and 26 nm in hydrated potato (*Solanum tuberosum*) walls examined by atomic force microscopy (Kirby et al., 2006). Given the dimensions of CMFs, these spacings give VFs of 1% to 2%, although much higher values may exist in other wall types, such as the polylamellate walls of celery (*Apium graveolens*) collenchyma, where x-ray diffraction estimates spacings as low as 5 nm (Kennedy et al., 2007a).

Percentage Composition by Weight of the CHC Network

Reported values for the weight percentage of HCs and cellulose in primary walls vary widely (Rose, 2003), probably reflecting differences in species, cell types, and physiological state of the samples analyzed.

HC M_r and Length

WallGen uses HC M_r to calculate how many HC molecules to generate and requires a value for HC length to place the HC ends in relation to the chain's midpoint when each HC is generated. This length will define the maximum permitted length of HC beam elements in the subsequent mechanical analysis, although in practice, most cross-bridges will be shorter because most HCs intersect two CMFs that are much closer together (Fig. 3A). The HC length should not exceed the contour length of a molecule of the chosen M_r, and that length will of course depend on the covalent structure of the HC being represented. For xyloglucans (XGs), the dominant HC in dicot primary walls, measured values for M_r range from approximately 10^5 to 10^6 using size exclusion chromatography (Rose, 2003), giving glucan backbones of approximately 148 to 1,480 nm (assuming Glc:Xyl:Gal:Fuc of 4:3:1:0.25 and 0.5 nm per Glc residue). This overlaps the range of lengths seen by electron microscopy (30–700 nm in onion; McCann et al., 1990).

Elastic Moduli of CMFs and HCs

These moduli define the mechanical properties of the virtual wall's two beam element types. The values, therefore, relate to properties of the individual HC chain or CMF and not to the more familiar (and usually much lower) moduli measured for the materials formed when many HCs or CMFs assemble into a film or other material.

Theoretical estimates for the modulus of fully crystalline cellulose (Tanaka and Iwata, 2006) are 130 to 160 GPa, a range consistent with measured deformations of the crystal lattice under load (Sakurada et al., 1962). The low crystallinity of primary wall cellulose (Lai-Kee-Him et al., 2002) will reduce stiffness to an uncertain but probably substantial degree (Eichhorn and Young, 2001).

Atomic force spectroscopy measures the mechanical properties of polymer chains such as HCs. The similar force-extension curves of several substituted or branched β-1,4 glucans (Li et al., 1999) suggest that their properties will be representative of XGs (a β-1,4 glucan with oligosaccharide side chains). Like most polymers, β-1,4 glucans show low stiffness as the folded polymer is initially extended, followed by rapidly rising stiffness as the chain is pulled taut and forces must distort covalent bonds to further stretch the extended chain (Li et al., 1999). The spring constant rises to greater than 10 pN pm^{-1}, suggesting that the stiffness of the extended β-1,4 glucan chain is comparable to that of a CMF. Such a high modulus may surprise biologists accustomed to think of "strong" CMFs and "weak" HCs, but HCs are not weak because of properties intrinsic to the HC chain. (The XG backbone is, after all, β-1,4-glucan just like cellulose.) Rather, they appear weak, first, because some HCs will not initially be fully extended; second, because the mechanically important glucan backbone occupies only a low VF in the wall; and third, because HCs bond to CMFs through weak H bonds that break ("peel") under load (Morris et al., 2004). In using linear elastic properties for the HCs in this study, we selected values lying between the very low values expected for nonextended chains and the high values expected for fully extended chains. We then imposed only very small extensions on the wall fragments (normally approximately 0.4%), so that, even if working with more realistic nonlinear properties, only small changes in modulus would be expected as a result of the displacements.

Conducting the Experiments

General Conditions

WallGen's design potentially allows wide scope to vary wall structure and the mechanical analyses performed. For all experiments reported, x and y dimensions for the wall fragments were 9.6 μm and walls had four layers containing CMFs, each of which was modeled as a square beam element with sides of 3.2 nm. CMF lengths were specified with a SD of 0.01 μm. When a VF was chosen, the average spacing between CMFs was estimated for a lattice of parallel and uniformly spaced CMFs. That average value was used to set the inter-layer spacing for the run. HCs were modeled as square beam elements with sides of 0.5 nm, and for purposes of length and M_r, they were considered to be XGs.

Imposed displacements were 0.4% of the initial wall length, and for each network generated, displacements

were imposed in two orthogonal directions by conducting two separate simulations. The two experiments provided E_{11}, the elastic modulus measured parallel to the CMFs in layer 1 (Fig. 2), and E_{22}, the modulus measured perpendicular to those CMFs. Analyses involved up to 2.5 million elements, 4.5 million nodes, and 18 million degrees of freedom. Each analysis was run using up to four processors to carry out element operations in parallel on a supercomputer and typically took 2.5 h to complete. WallGen's stochastic assembly of the CHC network means that each network generated with the same input settings differed in detailed microstructure. SE values in predicted mechanical properties for walls constructed with the same input settings were less than 5% for fragments of the size used.

Multinet Walls

The main set of simulations analyzed multinet walls, one of various wall types microscopists recognized by the characteristic changes in CMF alignments seen through the thickness of the wall (Roelofsen, 1959; Wardrop, 1962). Multinet walls are typically thin (approximately 0.1 μm), with only about four layers of CMFs (McCann and Roberts, 1991), and surround many internal parenchyma cells. In elongated organs, CMFs deposited at the inner surface of multinet walls run circumferentially around the cell, perpendicular to the organ's major growth axis (Roelofsen, 1959; Wardrop, 1962; Green et al., 1970; Sugimoto et al., 2000; Refregier et al., 2004). As growth increases wall area, the initial layers of CMFs collapse into each other (wall thinning by Poisson effect), but continued synthesis maintains overall wall thickness by adding CMFs at the wall's inner surface, displacing the original CMFs toward its outer surface. As individual CMFs move outward along the z axis, the strain they experience realigns them from transverse toward longitudinal so that they form a network on the outer surface that is random or even biased toward longitudinal. Theory predicts that strain realignment will be limited until CMFs reach the wall's outer regions (Erickson, 1980; Preston, 1982), so we used SD values of 0.1, 0.2, 0.3, and 1.5 rad for CMF alignments in layers one to four of our virtual multinet walls (Fig. 2; layer 1, with its well-aligned CMFs, represents the layer adjacent to the plasma membrane).

Exploring Multiple Input Variables

In experimental situations with many variables, the biologist's conventional experimental design fixes all variables except one, an approach that, if applied here, would require numerous experiments to investigate the influence of WallGen's user-defined variables. To provide an overview of the major effects of some variables from many fewer experiments, we employed "design of experiment" methods (Fowlkes and Creveling, 1995). This alternative to single-factor experimental plans identifies the major effects of different variables by the rational selection of a subset of combinations from the numerous possible combinations of variables that exist. Experiments to determine mechanical properties were planned by employing orthogonal arrays using three levels for each of four variables (CMF length, CMF VF, relative cross-bridge number [varied by changing HC M_r], and HC elastic modulus). Inspection of Table II will show the structured distribution of values (low, medium, and high) for each of the four variables among the 27 experiments.

Predicted Elastic Moduli

We first compared WallGen's predictions for E_{11} of a simple CHC network with that calculated using the "rule of mixtures," a well-established analytical method to approximate various material properties of composite and other materials on the basis of the elastic modulus and the VF each component occupies.

$$E_{11} = E_{CMF}V_{CMF} + E_{HC}V_{HC} + E_{matrix}V_{matrix}$$

CMFs (elastic modulus E_{CMF} = 30 GPa, V_{CMF} = 0.01) were highly aligned and orthogonal to the HCs (10 GPa, 0.0004) in all four layers of this network. CMFs extend throughout the full length of the layers to form a structure similar to a long-fiber-reinforced composite. FEA using WallGen predicts E_{11} = 318 MPa, less than 5% different from the value (304 MPa) determined using the rule of mixtures if we assume no matrix, so that $E_{matrix} = V_{matrix} = 0$.

Figure 2 illustrates the general appearance of the multinet walls analyzed. As expected given the linear elastic properties given to the CMFs and XGs, stress-strain curves for the virtual walls were linear up to the maximum strain tested (6.67%). To minimize inaccuracy while using linear elastic inputs, imposed strains were kept small (0.42%; 40-nm imposed displacements with x and y dimensions of 9.6 μm). Within the "design space" explored in 27 multinet walls selected by the design of experiments methodology, E_{11} (the elastic modulus in the direction parallel to the CMFs in layer 1) ranged from 40 to 405 MPa, E_{22} (the elastic modulus in the direction perpendicular to that of E_{11}) ranged from 0.7 to 41 MPa, and mechanical anisotropy (E_{11}/E_{22}) ranged from 8 to 61 (Table II; Fig. 4). (In the context of multinet walls in an internode or root, E_{11} measures stiffness transverse to the organ long axis, whereas E_{22} measures stiffness parallel to the organ long axis and so along its major growth direction.) To see how each input variable influenced E_{11} and E_{22}, we used major effect plots and analysis of means (Fowlkes and Creveling, 1995; Fig. 5A). None of these four input factors raised E_{11} while lowering E_{22} or vice versa, so that any anisotropy changes (Fig. 5B) reflected differences in the relative magnitude of changes in the two moduli. Three of the input factors acted similarly on the two moduli: increased CMF length, CMF VF, and

Table II. *Elastic moduli for 27 multinet walls predicted using WallGen and finite element analysis and using an orthogonal L27 array providing three input levels for each of four input factors.*

Experiment No.	Inputs[a]				Predicted Properties of Wall		
	CMF Length	HC M_r	CMF VF	HC Elastic Modulus	E_{11}	E_{22}	E_{11}/E_{22}
	μm	*×10³*		*GPa*	*MPa*	*MPa*	
1	4.0	200	0.015	1	137.8	11.4	12.1
2	4.0	200	0.020	5	297.6	28.7	10.4
3	4.0	200	0.025	10	405.0	41.7	9.7
4	4.0	400	0.015	5	130.2	7.8	16.7
5	4.0	400	0.020	10	219.9	15.1	14.5
6	4.0	400	0.025	1	109.9	6.6	16.7
7	4.0	800	0.015	10	72.6	1.6	45.4
8	4.0	800	0.020	1	40.8	0.7	61.6
9	4.0	800	0.025	5	110.9	2.4	46.4
10	5.0	200	0.015	5	220.7	24.2	9.1
11	5.0	200	0.020	10	335.4	38.1	8.8
12	5.0	200	0.025	1	303.7	26.5	11.5
13	5.0	400	0.015	10	183.5	13.0	14.1
14	5.0	400	0.020	1	135.4	7.0	19.3
15	5.0	400	0.025	5	290.8	20.1	14.5
16	5.0	800	0.015	1	48.3	1.3	38.6
17	5.0	800	0.020	5	119.6	3.9	30.5
18	5.0	800	0.025	10	167.4	4.1	40.5
19	6.0	200	0.015	10	249.6	26.0	9.6
20	6.0	200	0.020	1	244.8	23.1	10.6
21	6.0	200	0.025	5	370.6	41.6	8.9
22	6.0	400	0.015	1	134.7	8.1	16.5
23	6.0	400	0.020	5	236.5	16.6	14.2
24	6.0	400	0.025	10	343.6	27.7	12.4
25	6.0	800	0.015	5	101.7	2.8	36.2
26	6.0	800	0.020	10	161.1	4.1	38.9
27	6.0	800	0.025	1	110.0	2.8	40.0

[a]Other user-defined inputs were as follows: size 9.6 × 9.6 μm; four layers; elastic modulus of CMFs = 30 GPa; weight percentage for HCs = 36%; SD for CMF orientation of 0.1, 0.2, 0.3, and 1.5 rad in layers 1 to 4, respectively.

HC elastic modulus stiffened walls in both directions (Fig. 4A) with little change in anisotropy (E_{11}/E_{22}; Fig. 5B). In contrast, reducing relative cross-bridge number strongly increases anisotropy (Fig. 5B), because E_{22} decreases proportionally more than E_{11} does. That is, stiffness parallel to the major growth axis would fall relatively more than would stiffness measured at right angles to it. Importantly, however, most of this rise occurs in walls in which E_{22} is low (Fig. 4B).

To see how different degrees of CMF alignment influence mechanical properties and to shed light on how the different CMF orientations in the layers within the multinet wall might contribute to the wall's overall mechanics, we modeled walls having four identical layers. CMF alignments were varied from parallel (SD = 0) to random (SD ≥ 1.5 rad). Relaxing CMF alignment by increasing the SD converts a mechanically highly anisotropic wall (E_{11}/E_{22} of approximately 2,800 when SD = 0.1 rad) into an isotropic wall by enormously increasing E_{22} while gradually lowering E_{11} about 2-fold until E_{11} and E_{22} converge at about 50 MPa with the other settings used in this example (Fig. 6).

DISCUSSION

We have described software that builds CHC networks intended to provide one-to-one correspondence between mechanical elements in the real and virtual walls. Predicted small displacement mechanical properties for 9.6- × 9.6-μm fragments, a size large enough to be relevant to cell shape determination, are based on inputs that concern only wall polymers, either individually or as populations. Those predicted values overlap the range of measured values. Predictions of the mechanical effects of changing wall structure on wall mechanics are relatively rapid and quantitative.

Inputs and Assumptions

Any modeling exercise depends on using appropriate inputs and making reasonable assumptions in the operation of the model. Inputs were based on a review of experimental data, and all biological experience points to there probably being considerable variation within species (cell type, developmental stage, etc.) and between species in the features represented by

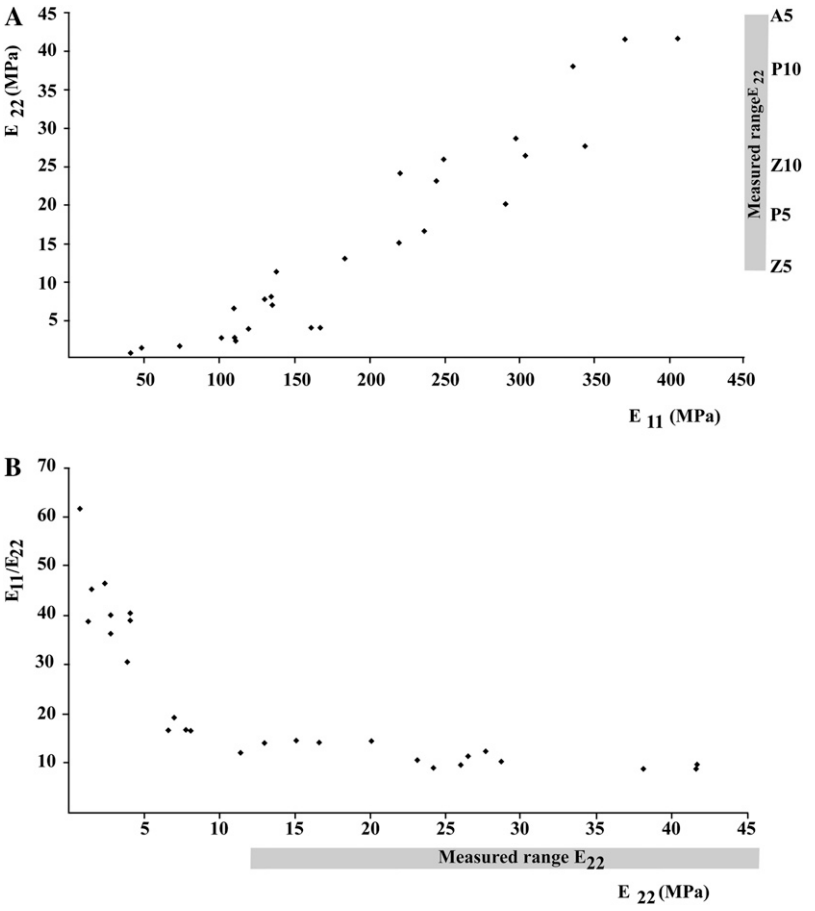

Figure 4. A, Scatterplot showing E_{11} and E_{22} for the 27 walls detailed in Table II. Measured values for E_{22} of *Zea* (Z), *Populus* (P), and *Aristolochia* (A) are shown on the E_{22} axis after correcting upward by factors of 5 and 10 (Z5, Z10, etc.) as described in the text. Some measured values for E_{22} exceed the range covered by this graph. B, Scatterplot showing E_{22} and E_{11}/E_{22} for the same walls. E_{11}/E_{22} rises gently as E_{22} falls over the range of experimentally measured values but rises sharply as E_{22} falls below the range of measured values.

those inputs. Therefore, it is almost certainly misleading to think of there being one correct value for any of the inputs, but it is nevertheless important to use inputs within the in vivo range. However, the consequences of many inaccuracies are obvious; if we underestimate VF, elastic moduli, or CMF length, we will underestimate E_{11} and E_{22}.

The well-supported assumption underlying all multiscale modeling is that proper representation of microstructure and its mechanics enables prediction of larger scale mechanical properties. Important assumptions in our case are that CMFs are located in a series of well-defined layers, that all HCs form a single cross-bridge between two CMFs, and that the complex mechanical properties of HC cross-bridges can, when modeling small displacements, be approximated by giving them linear elastic properties. None of these assumptions are essential features of the model. In particular, the mechanical elements in FEA can be given much more complex properties than those we used. Nonlinear elastic properties, for example, will more accurately depict how a polymer chain behaves when pulled taut (Li et al., 1999), and FEA techniques such as those applied to bond failure and microcrack initiation and propagation have potential application in modeling the separation of HCs from CMFs during further extension.

Predicted Versus Experimental Measurements

Virtual multinet walls with the range of input values we applied have E_{11} predicted to range from 41 to 405 MPa, E_{22} from 0.7 to 42 MPa, and E_{11}/E_{22} from 8 to 61. Comparing predicted with measured properties turns out to be far from straightforward. Reported values are 3.7 MPa (Park et al., 2004) and 8 to 10 MPa (Kohler et al., 2000) for the youngest measurable internodes of poplar (*Populus alba*) and winding liana (*Aristolochia macrophylla*), respectively, 1 to 4 MPa for mesocotyls of maize (*Zea mays*; Schopfer et al., 2001), and 21 to 28 MPa (Ryden et al., 2003) for Arabidopsis (*Arabidopsis thaliana*) hypocotyls. While these all fall within the range of values WallGen predicts for E_{22} of multinet walls, such a direct comparison is not valid. First, experimental measurements are expressed per unit of tissue area (which might be 10- to 20-fold higher than the wall area basis we use). Second, they are for intact walls, which, for dicot walls (Ryden et al., 2003), might be about twice as stiff as the CHC network alone that we are considering. This suggests that measured values should be corrected upward by factors of 5 or 10, and we included the corrected values for *Populus*, *Aristolochia*, and *Zea* in the scatterplot of WallGen's E_{22} predictions (Fig. 4A). There is substantial overlap between predicted values and these corrected mea-

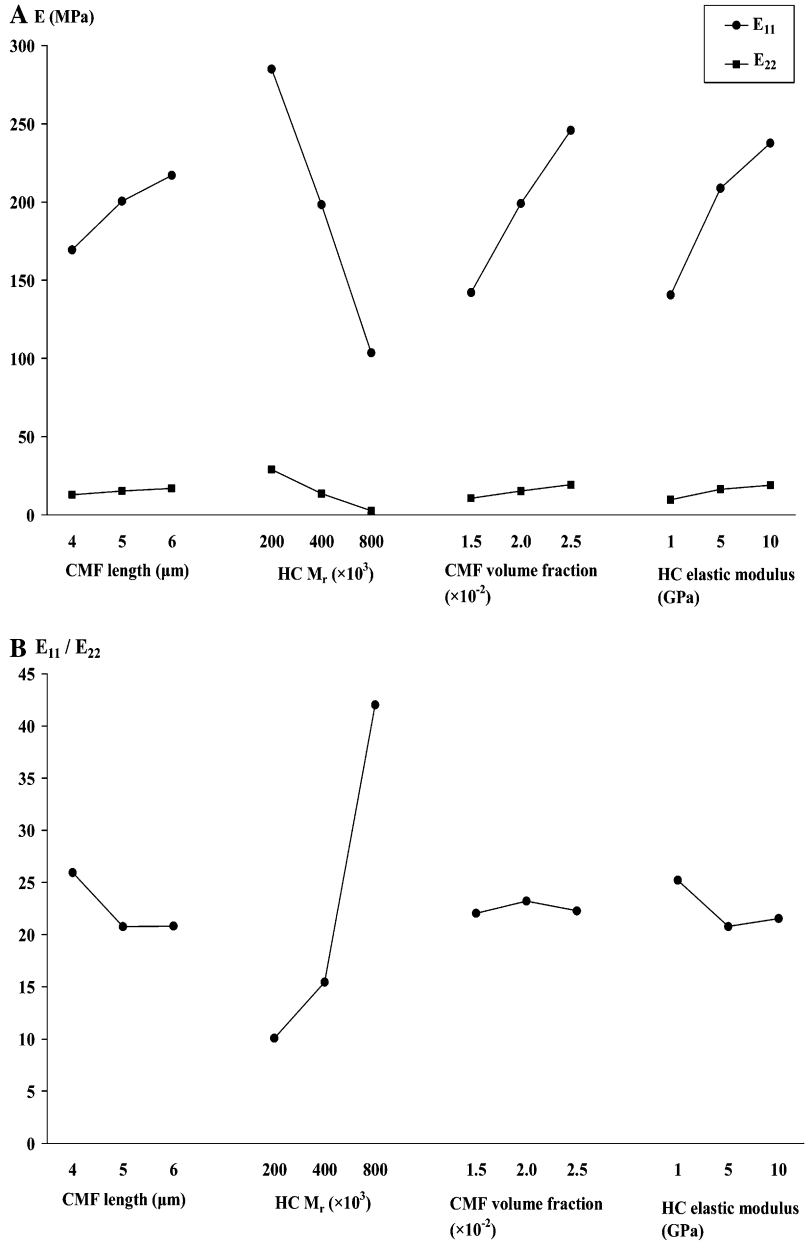

Figure 5. Major effect/analysis of means for the data collected in Table II. A, Plots for E_{11} and E_{22}, the predicted elastic moduli parallel and perpendicular to the aligned CMFs in layer 1. B, Plots for mechanical anisotropy (E_{11}/E_{22}).

sured values but not with the substantially higher figures of Ryden et al. (2003) for Arabidopsis hypocotyl (125 or 250 MPa after correction).

Consideration of the data in Figure 4A shows that 13 of 27 walls have E_{22} in the measured range containing the corrected values, and with the exception of the relative number of HC cross-bridges, which must be set to either the medium or high value, walls giving E_{22} in the measured range can have the other three variables (CMF length, VF, and HC modulus) set to our low, medium, or high values. Predicted properties in the measured range, therefore, are far from being dependent on all inputs being set to high, and for the most part it is combinations of input values that place walls in or below the measured range.

Before leaving the comparison with measured values, it is worth noting that experimental measurements all describe the mechanics of complex organs to whose mechanical properties very diverse walls contribute in unknown proportions. Internal cells are themselves a mixture of those with thin multinet walls similar to those we model and cells with thicker walls and differently arranged CMFs (Kohler et al., 2000; Derbyshire et al., 2007). Of probably greater importance, however, are the mechanical properties of the thick outer epidermal wall. These are widely believed to dominate the whole internode's mechanical properties in so far as they control growth rates (Kutschera and Niklas, 2007). Removing the thick epidermal wall promotes elongation growth of internal tissues, sug-

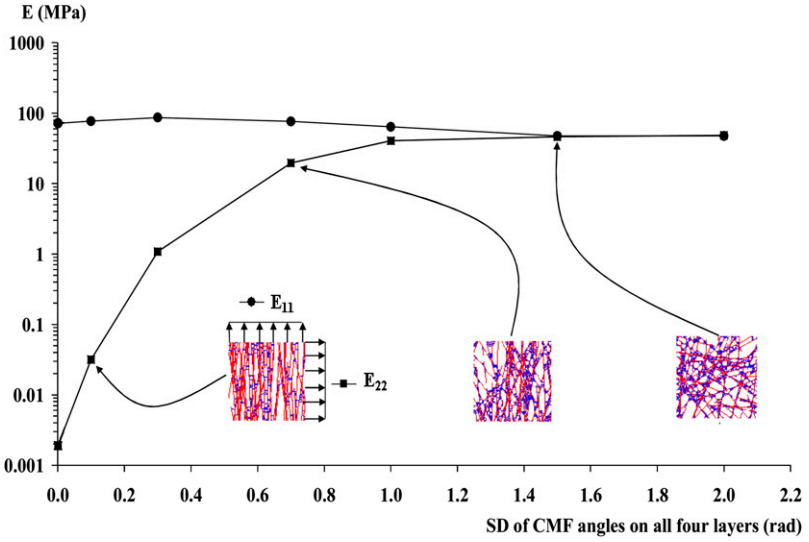

Figure 6. Plot of E_{11} and E_{22} versus CMF orientation in walls with four identical layers. The three panels give views of one layer of a wall constructed with CMFs having the mean and SD indicated by the arrows to points on the graph. The left panel shows the direction in which displacements are applied to determine E_{11} and E_{22}.

gesting that their walls (many with multinet architecture) are more extensible but that the stiffer epidermal wall restrains their expansion when the internode is intact. One obvious reason for the epidermal wall being stiff is that the CMFs in its helicoidal or other polylamellate structure may have net longitudinal alignment (Suslov and Verbelen, 2006), whereas CMFs have net transverse alignment in multinet walls of internal cells. Therefore, when external loads are applied to mechanically characterize an internode, E_{11} is the relevant modulus for the thick epidermal wall with longitudinal CMFs, whereas the much lower E_{22} is relevant for the thin multinet walls of internal cells. The modulus for longitudinal loading of isolated onion epidermis is as high as 728 MPa expressed on a wall area basis (Hepworth and Bruce, 2004). This single, externally facing wall, therefore, may substantially raise the overall modulus that is measured when an internode is loaded longitudinally and perhaps contribute to taking some experimentally measured values beyond the range of our predicted values, which are for thin multinet walls alone.

All the virtual multinet walls we examined are mechanically anisotropic (E_{11}/E_{22} from 8 to 61), as expected for walls growing mainly in the direction described by E_{22}. Direct measurements of mechanical anisotropy are available for the thick walls of giant cells of the alga *Nitella opaca*. These have mechanical and growth anisotropies of about 5 (Probine and Preston, 1962). Although *Nitella* walls have multinet architecture, their HC chemistry and their HC-CMF bonding remains unknown. Their massive thickness makes it difficult to compare their mechanical properties directly with our current predictions for much thinner walls.

In summary, measured and predicted values for E_{22} show considerable overlap, and walls showing those realistic mechanical properties do not rely on all inputs being set to the highest levels we investigated but rather on having an appropriate combination of traits. Given that experimental measurements are made on complex tissues with, for example, stiff outer epidermal walls, experimental measurements are more likely to produce higher values than appropriate for the multinet walls we are modeling, making the match particularly good. The Poisson ratio for multinet walls also shows the relationship with E_{11} and E_{22} that is expected from the theory of anisotropic materials (H. Kha, S. Kalyanasundaram, and R.E. Williamson, unpublished data).

Mechanical Responses to Input Values

WallGen's capacity to predict how different input values affect wall mechanics is of interest in two contexts. First, during development and when responding to environmental changes, the plant may regulate physiological processes affecting wall structure and composition and so change parameters that form inputs to WallGen (e.g. polymer weight percentages, HC M_r, CMF orientation). Second, the correct numerical values for some inputs (HC modulus, CMF VF) are particularly uncertain, making it valuable to explore how strongly those uncertainties might affect predicted wall properties.

The low, medium, and high settings for the four variables used in the 27 simulations in Table II were selected to enable each variable's effects to be identified by analysis of means and major effect plots. Changes in CMF length, CMF VF, and HC elastic modulus all change wall mechanics in the expected directions. That is, giving walls longer or additional CMFs makes them stiffer, as does giving them less readily extensible HCs. A 10-fold increase in HC stiffness increases E_{11} and E_{22} only by factors of 1.7 and 2.0, respectively. This is consistent with the intuitive view that HCs would contribute more to E_{22} (i.e. to stiffness perpendicular to the direction of CMFs in

layer 1) than they would to E_{11}, but the effect is relatively slight. Given that HC modulus is one of the more uncertain parameters that WallGen uses, the finding that even 10-fold changes in modulus produce 2-fold or smaller changes in wall elastic modulus is reassuring regarding the robustness of WallGen predictions. We consider below why E_{22} responds only slightly more than E_{11} so that wall mechanical anisotropy changes only slightly.

The effects of increasing the relative number of cross-bridges exceed the effects seen with the other three variables. The greater effect on E_{22} than on E_{11} raises mechanical anisotropy (E_{11}/E_{22}) almost 5-fold for a 4-fold decrease in relative cross-bridge number. In our example where we change HC M_r, the effect on relative cross-bridge number depends on our assumption that each HC molecule forms only one cross-bridge, so that increasing the notional M_r of the HC reduces the number of cross-bridges if the HC weight percentage is kept constant. The data of Pauly et al. (1999) on the average size of H-bonded regions can be interpreted to indicate that the XGs they studied (M_r 100,000) form only a single cross-bridge. To our knowledge, however, no comparable experimental evidence is available to show how many cross-bridges form from XG chains with higher M_r. The magnitude of the HC M_r effect would be reduced if they form more than one or even reversed if high-M_r XGs form more cross-bridges per unit length of chain than do low-M_r XG. Plotting anisotropy as a function of E_{22} in a scatterplot (Fig. 4B) shows that, with our assumptions, taking relative cross-bridge number low enough to strongly raise anisotropy reduces E_{22} below the range of measured values (approximately 12 MPa after correction), raising questions about the effect's importance in vivo.

General Features of Multinet Walls

Multinet wall architecture shows a gradual reduction in the precision of CMF alignment between the wall's inside and outside surfaces (layers 1 and 4 in WallGen). The mechanics of walls constructed with four layers sharing identical CMF orientations show the large changes resulting from rearranging highly aligned CMFs into randomly oriented CMFs (Fig. 5). The more than 1,000-fold increase in E_{22} enormously exceeds the relatively modest falls in E_{11}, so that mechanical anisotropy falls from about 2,800 to 1. If these provide some guide to the properties of the individual layers in our standard multinet wall (SD of 0.1, 0.2, 0.3, and 1.5 rad), we can expect in moving from layer 1 to layer 4 to see large increases in E_{22} with relatively small falls in E_{11}. On this view, the poorly aligned CMFs in layer 4 will contribute significantly to the wall's overall E_{22}, which, if it depended only on the inner layers, would be extremely low. A view of CMFs dominating E_{11} and HCs dominating E_{22}, therefore, is too simplistic for multinet walls, but the fact that changing the relative number of cross-bridges does change anisotropy indicates that a differential contribution of HCs to the two moduli remains. The very large increases in E_{22} with relaxation of CMF alignment suggest that alignment changes will be a powerful route to adjust anisotropy in multinet walls, an effect we explore in more detail elsewhere (H. Kha, S. Kalyanasundaram, and R. Williamson, unpublished data).

In conclusion, we have described the use of WallGen to predict the mechanical properties of a CHC network of the type proposed for primary cell walls. There is satisfactory overlap between predicted and measured values that is not dependent on choosing uniformly high input values, and some higher measured values may be influenced by other wall types, notably the thick epidermal wall. Predictions require explicit specification of wall structure and polymer mechanics, potentially allowing exploration of further variants of multinet architecture, since the view that HCs cross-bridge CMFs is not universally accepted. Our analyses were confined to multinet walls, but WallGen, with its ability to specify any combination of alignments in successive layers, can potentially explore other wall types, such as polylamellate and helicoidal. Fully representing such walls provides computational challenges, since they will require many more wall layers (wall thicknesses of several μm rather than 0.1 μm) and probably much higher VFs if polylamellate collenchyma are typical (Kennedy et al., 2007a). Future refinements to WallGen will try to capture the mechanical properties of the HCs and their interactions with CMFs with more accuracy than the current linear elastic model.

ACKNOWLEDGMENTS

We thank the Australian Partnership for Advanced Computing for the use of their supercomputing facilities, including Abaqus, and the Information Technology staff at the Department of Engineering (Australian National University) for their assistance in the installation of the HyperWorks system. We thank Prof. D.C. Stahl for helpful advice in the early stages of this project.

Received September 1, 2009; accepted November 15, 2009; published December 9, 2009.

LITERATURE CITED

Allen KB, Sasoglu FM, Layton BE (2009) Cytoskeleton-membrane interactions in neuronal growth cones: a finite analysis study. J Biomech Eng **131:** 021006

Altaner CM, Jarvis MC (2008) Modelling polymer interactions of the 'molecular Velcro' type in wood under mechanical stress. J Theor Biol **253:** 434–445

Baskin TI (2005) Anisotropic expansion of the plant cell wall. Annu Rev Cell Dev Biol **21:** 203–222

Bergander A, Salmén L (2002) Cell wall properties and their effects on the mechanical properties of fibers. J Mater Sci **37:** 151–156

Bolduc JF, Lewis L, Aubin CE, Geitmann A (2006) Finite-element analysis of geometrical factors in micro-indentation of pollen tubes. Biomech Model Mechanobiol **5:** 227–236

Carpita NC, Gibeaut DM (1993) Structural models of primary cell walls in flowering plants: consistency of molecular structure with the physical properties of the walls during growth. Plant J **3:** 1–30

Chamis CC, Sendeckyj GP (1968) Critique on theories predicting thermoelastic properties of fibrous composites. J Compos Mat **2:** 332–358
Davies LM, Harris PJ (2003) Atomic force microscopy of microfibrils in primary cell walls. Planta **217:** 283–289
Derbyshire P, Findlay K, McCann MC, Roberts K (2007) Cell elongation in Arabidopsis hypocotyls involves dynamic changes in cell wall thickness. J Exp Bot **58:** 2079–2089
Eichhorn SJ, Young RJ (2001) The Young's modulus of a microcrystalline cellulose. Cellulose **8:** 197–207
Erickson RO (1980) Microfibrillar structure of growing plant cell walls. Lect Notes Biomath **33:** 192–212
Fowlkes WY, Creveling CM (1995) Engineering Methods for Robust Product Design: Using Taguchi Methods in Technology and Product Development. Addison-Wesley, New York
Franke WW, Ermen B (1969) Negative staining of plant slime cellulose: an examination of the elementary fibril concept. Z Naturforsch [B] **24:** 918–922
Green PB, Erickson RO, Richmond PA (1970) On the physical basis of cell morphogenesis. Ann N Y Acad Sci **175:** 712–731
Hansson MT, Rasmuson A (2004) Finite element analysis of three dimensional fibre networks. Nord Pulp Pap Res J **19:** 105–111
Hayashi T (1989) Xyloglucans in the primary cell wall. Annu Rev Plant Physiol Plant Mol Biol **40:** 139–168
Hepworth DG, Bruce DM (2004) Relationships between primary plant cell wall architecture and mechanical properties for onion bulb scale epidermal cells. J Texture Stud **35:** 586–602
Hofstetter K, Hellmich C, Eberhardsteiner J (2005) Development and experimental validation of a continuum micromechanics model for the elasticity of wood. Eur J Mech Solid **24:** 1030–1053
Keckes J, Burgert I, Fruhmann K, Muller M, Kolln K, Hamilton M, Burghammer M, Roth S, Stanzl-Tschegg S, Fratzl P (2003) Cell-wall recovery after irreversible deformation of wood. Nat Mater **2:** 810–814
Kennedy CJ, Cameron GJ, Sturcová A, Apperley DC, Altaner C, Wess TJ, Jarvis MC (2007a) Microfibril diameter in celery collenchyma cellulose: x-ray scattering and NMR evidence. Cellulose **14:** 235–246
Kennedy CJ, Sturcová A, Jarvis MC, Wess TJ (2007b) Hydration effects on spacing of primary-wall cellulose microfibrils: a small angle X-ray scattering study. Cellulose **14:** 401–408
Kha H, Tuble S, Kalyanasundaram S, Williamson RE (2008) Finite element analysis of plant cell wall materials. Frontiers in Materials Science and Technology **32:** 197–201
Kirby AR, Ng A, Waldron KW, Morris VJ (2006) AFM investigations of cellulose fibers in bintje potato (*Solanum tuberosum* L.) cell wall fragments. Food Biophys **1:** 163–167
Kohler L, Speck T, Spatz HC (2000) Micromechanics and anatomical changes during early ontogeny of two lianescent *Aristolochia* species. Planta **210:** 691–700
Kutschera U, Niklas KJ (2007) The epidermal-growth-control theory of stem elongation: AN old and a new perspective. J Plant Physiol **164:** 1395–1409
Kwon YW, Kwon YW, Allen DH, Talreja R, editors (2008) Multiscale Modeling and Simulation of Composite Materials. Springer, New York
Lai-Kee-Him J, Chanzy H, Muller M, Putaux JL, Imai T, Bulone V (2002) *In vitro* versus *in vivo* cellulose microfibrils from plant primary wall synthases: structural differences. J Biol Chem **277:** 36931–36939
Li H, Rief M, Oesterhelt F, Gaub HE, Zhang X, Shen J (1999) Single-molecule force spectroscopy on polysaccharides by AFM: nanomechanical fingerprint of alpha-1,4 -linked polysaccharides. Chem Phys Lett **305:** 197–201
McCann M, Wells B, Roberts K (1990) Direct visualization of cross-links in the primary plant cell wall. J Cell Sci **96:** 323–334
McCann MC, Roberts K (1991) Architecture of the primary cell wall. *In* CW Lloyd, ed, The Cytoskeletal Basis of Plant Growth and Form. Academic Press, London, pp 109–129
Morris S, Hanna S, Miles MJ (2004) The self-assembly of plant cell wall components by single molecule force spectroscopy and Monte Carlo modelling. Nanotechnology **15:** 1296–1301
Park YW, Baba K, Furuta Y, Ida I, Sameshima K, Arai M, Hayashi T (2004) Enhancement of growth and cellulose accumulation by overexpression of xyloglucanase in poplar. FEBS Lett **564:** 183–187
Pauly M, Albersheim P, Darvill A, York WS (1999) Molecular domains of the cellulose/xyloglucan network in the cell walls of higher plants. Plant J **20:** 629–639
Preston RD (1974) The Physical Biology of Plant Cell Walls. Chapman and Hall, London
Preston RD (1982) The case for multinet growth in growing walls of plant cells. Planta **155:** 356–363
Probine MC, Preston RD (1962) Cell growth and the structure and mechanical properties of the wall in internodal cells of *Nitella opaca*. II. Mechanical properties of the walls. J Exp Bot **13:** 111–127
Refregier G, Pelletier S, Jaillard D, Hofte H (2004) Interaction between wall deposition and cell elongation in dark-grown hypocotyl cells in Arabidopsis. Plant Physiol **135:** 959–968
Roelofsen PA (1959) The plant cell wall. Handbuch der Pflanzenatomie **III:** 4
Rose JKC (2003) The Plant Cell Wall: Annual Plant Reviews, Vol 8. CRC Press, Oxford
Ryden P, Sugimoto-Shirasu K, Smith AC, Findlay K, Reiter WD, McCann MC (2003) Tensile properties of Arabidopsis cell walls depend on both a xyloglucan cross-linked microfibrillar network and rhamnogalacturonan II-borate complexes. Plant Physiol **132:** 1033–1040
Sakurada I, Nukushina Y, Ito T (1962) Experimental determination of the elastic modulus of crystalline regions in oriented polymers. J Polymer Sci **57:** 651–660
Salmén L (2004) Micromechanical understanding of the cell-wall structure. C R Biologies **327:** 873–880
Schaap IA, Carrasco C, de Pablo PJ, MacKintosh FC, Schmidt CF (2006) Elastic response, buckling, and instability of microtubules under radial indentation. Biophys J **91:** 1521–1531
Schopfer P, Lapierre C, Nolte T (2001) Light-controlled growth of the maize seedling mesocotyl: mechanical cell-wall changes in the elongation zone and related changes in lignification. Physiol Plant **111:** 83–92
Smith AE, Moxham KE, Middelberg APJ (1998) On uniquely determining cell-wall material properties with the compression experiment. Chem Eng Sci **53:** 3913–3922
Sprey B, Bochem HP (1993) Formation of cross-fractures in cellulose microfibril structure by an endoglucanase-cellobiohydrolase complex from *Trichoderma reesei*. FEMS Microbiol Lett **106:** 239–243
Stahl DC, Cramer SM, Geimer RL (1997) Effects of microstructural heterogeneity in cement excelsior board. Wood Fiber Sci **29:** 345–352
Stahl DC, Kramer SM (1998) A three-dimensional network model for a low density fibrous composite. J Eng Mater Technol **120:** 126–130
Sugimoto K, Williamson RE, Wasteneys GO (2000) New techniques enable comparative analysis of microtubule orientation, wall texture and growth rate in intact roots of *Arabidopsis thaliana*. Plant Physiol **124:** 1–15
Suslov D, Verbelen JP (2006) Cellulose orientation determines mechanical anisotropy in onion epidermis cell walls. J Exp Bot **57:** 2183–2192
Tanaka F, Iwata T (2006) Estimation of the elastic modulus of cellulose crystal by molecular mechanics simulation. Cellulose **13:** 509–517
Thompson DS (2005) How do cell walls regulate plant growth? J Exp Bot **56:** 2275–2285
Wardrop AB (1962) Cell wall organisation. I. The primary wall. Bot Rev **28:** 241–285
Wasteneys GO (2004) Progress in understanding the role of microtubules in plant cells. Curr Opin Plant Biol **7:** 651–660
Whitney SEC, Gothard MGE, Mitchell JT, Gidley MJ (1999) Roles of cellulose and xyloglucan in determining the mechanical properties of primary plant cell walls. Plant Physiol **121:** 657–664
Zykwinska AW, Ralet MC, Garnier CD, Thibault JF (2005) Evidence for in vitro binding of pectin side chains to cellulose. Plant Physiol **139:** 397–407